COMMUNICATION

Check for updates

Ligand solid-solution tuning of magnetic and mechanical properties of the van der Waals metal–organic magnet NiCl$_2$(btd)$_{1-x}$(bod)$_x$†

Emily Myatt, [iD] [a] Simrun Lata,[a] Jem Pitcairn, [iD] [a] Dominik Daisenberger,[b] Silva M. Kronawitter, [iD] [c] Sebastian A. Hallweger, [iD] [c] Gregor Kieslich, [iD] [c] Stephen P. Argent, [iD] [a] Jeremiah P. Tidey [iD] [d] and Matthew J. Cliffe [iD] *[a]

Van der Waals (vdW) magnets offer unique opportunities for exploring magnetism in the 2D limit. Metal–organic magnets (MOM) are of particular interest as the functionalisation of organic ligands can control their physical properties. Here, we demonstrate tuning of mechanical and magnetic function of a noncollinear vdW ferromagnet, NiCl$_2$(btd) (btd = 2,1,3-benzothiadiazole), through creating solid-solutions with the oxygen-substituted analogue ligand 2,1,3-benzoxadiazole (bod). We synthesise NiCl$_2$(btd)$_{1-x}$(bod)$_x$ up to x = 0.33, above which we find mixtures primarily composed of 1D NiCl$_2$(bod)$_2$. Magnetometry reveals bod incorporation reduces the coercivity significantly (up to 60%), without altering the ordering temperatures. High pressure synchrotron diffraction measurements up to 0.4 GPa demonstrate that the stiffest axis is the b axis, through the Ni−N−(O/S)−N−Ni bonds, and the softest is the interlayer direction. Doping with bod fine-tunes this compressibility, softening the layers, but stiffening the interlayer axis. This demonstrates that substitution of organic ligands in vdW MOMs can be used to realise targeted magnetic and mechanical properties.

The modularity of metal–organic materials means that compounds with identical structural topologies but different ligands can be readily synthesised (they are 'isoreticular').[1] This in turn enables the synthesis of diverse ligand solid-solutions,[2,3] which allows control of chemical function, *e.g.* methane separation[4] and catalytic activity.[5] The physical properties of metal–organic frameworks (MOFs), *e.g.* mechanical,[6] magnetic,[7] or electronic[8] function, can

equally be controlled through ligand solution. There remains a great deal to learn about the physical properties of mixed-ligand MOFs, especially the possibility of creating function beyond the linear combination of stoichiometric end-members.[9] Ligand solid-solutions in zeolitic imidazolate frameworks (ZIFs) subtly modulate the magnetic ordering temperatures of **sod** topology ZIFs[10] and control the pressure-induced pore closing ZIF-4 analogues;[11,12] and solid-solutions of terminal halide ligands in Cr(pyz)$_2$Br$_x$I$_{2-x}$ produce temperature-induced valence tautomeric transitions not present in the stoichiometric phases.[13]

Ligand solid-solution control over mechanical and magnetic function in vdW magnets is of special interest because pressure- and strain-control over magnetism can be readily achieved in devices.[14] This is particularly true for noncollinear magnets, where continuous evolution of magnetic order and properties is possible.[15] We have recently reported a family of new layered MOMs with noncollinear magnetic structures, including the canted ferromagnet NiCl$_2$(btd).[16] This material consists of NiCl$_2$ chains coordinated by the nitrogens of the nonlinear btd ligand to form corrugated sheets [Fig. 1]. The easy-axis ferromagnetic chains in combination with the tilting of chains induced by the ligand geometry leads to noncollinear canted ferromagnetism with significant coercive field, $\mu_0 H_c$ = 1.0(1) T.[16] The modularity of this
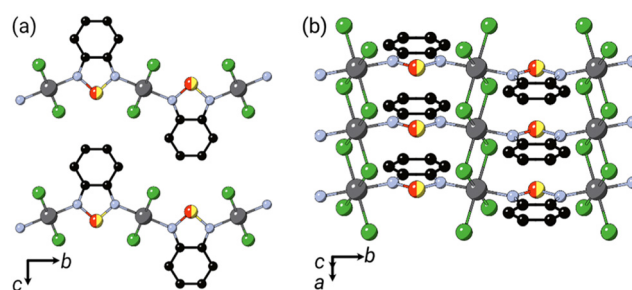
[a] School of Chemistry, University of Nottingham, University Park, Nottingham, NG7 2RD, UK. E-mail: matthew.cliffe@nottingham.ac.uk

[b] Diamond Light Source, Chilton, Didcot OX11 0DE, UK

[c] TUM Natural School of Sciences, Technical University of Munich, D-85748 Garching, Germany

[d] Department of Physics, University of Warwick, Gibbet Hill Road, Coventry, CV4 7AL, UK

Fig. 1 Structure of NiCl$_2$(btd)$_{1-x}$(bod)$_x$. (a) Viewed along the [100] direction (b) viewed along the [101] direction. C = black; Ni = grey; Cl = green; N = blue; O/S = red/yellow and H atoms omitted for clarity.

system, together with the promise of its magnetic function, prompted us to investigate whether we could use substitution of btd ligand for bod to not only alter the structure, but also tune the magnetic and mechanical properties of MOMs.

We showed that $NiCl_2(btd)$ can be made phase pure and crystalline through the direct reaction of $NiCl_2 \cdot 6H_2O$ and btd,[16] and thus we first explored this approach to create the solid-solutions $NiCl_2(btd)_{1-x}(bod)_x$, with target bod fraction, $x_t = 0$, 0.25, 0.5, 0.75 and 1.0 [Section S1, ESI†].

Analysis of the powder X-ray diffraction (PXRD) data confirmed that we were able to produce the desired phase up to $x_t \leq 0.75$ [Fig. 2 and Fig. S2, S3, ESI†]. We found that the pure bod phase did not form. Consequently, we synthesised a series through the reaction of ethanolic solutions of nickel chloride and ligands over the same target range of x_t, analogous to $CoCl_2(btd)$.[17] We found by analysis of PXRD data this again produced powders isostructural to $NiCl_2(btd)$ up to $x_t \leq 0.75$, but at $x_t = 1$ we obtained a phase mixture with an unknown primary phase. Pawley refinement showed that the samples synthesised through direct reaction contained very small quantities of starting material, but that the solution-synthesised samples had broader diffraction peaks, likely due to small particle sizes [Fig. S2 and Section S2.1, ESI†].

The phase mixture formed during solution synthesis with $x_t = 1$ included a number of small single crystals [Sections S2.3 and S2.4, ESI†]. We found using single crystal X-ray diffraction these to be a new 1D coordination polymer $NiCl_2(bod)_2$, containing trans-$NiCl_4N_2$ octahedra connected into $NiCl_2$ chains with terminal bod ligands [Section S2.3 and Fig. S15, S16, Table S5, ESI†], and a small number of crystals of $NiCl_2 \cdot 2H_2O$.[18] Re-analysis of our PXRD data in the light of this showed it was primarily $NiCl_2(bod)_2$ and a small quantity of nickel chloride hydrates. Further examination using single crystal electron diffraction (SCED) of the remainder of the reaction mixture revealed that the sample contained a number of different phases with unit cells closely related to $NiCl_2(btd)$, though with slightly different symmetries [Section S2.4 and Fig. S17–S20, Table S6, ESI†].[16] Comparison of refinements with only bod, only btd, and mixed ligands showed that these nanocrystals were monoclinic twinned $NiCl_2(bod)$ and an orthorhombic

polymorph of $NiCl_2(btd)$, although we cannot exclude that this orthorhombic phase includes a low proportion of bod ($<5\%$). We note these phases are not seen in the bulk PXRD and hence, we ascribe the formation of a small number of nanocrystals of $NiCl_2(btd)$ to the presence of adventitious btd, likely facilitated by its high vapour pressure [Fig. S4, ESI†]. This highlights the capability of SCED to find and solve the structures of even minor crystalline phases.

We determined the bod content by solution ^{1}H NMR, x_{NMR}, by dissolving the sample in DMSO-d_6. We found all samples to be bod-deficient. Together with the formation of $NiCl_2(bod)_2$ in preference to $NiCl_2(bod)$, this suggests that the more electron deficient bod does not coordinate as readily as the btd. This is further borne out by the lack of reported metal complexes containing bod as a ligand in the CSD. We found that the $x_{NMR} = 0.31$ ($x_t = 0.75$) solid-state sample was poorly crystalline and impure, so has not been further analysed. We thus focussed on samples with $x_t \leq 0.75$ for solution state sample and $x_t \leq 0.50$ for solid state samples.

Comparison of the Pawley derived unit cell volume and lattice parameters with the composition determined from NMR shows linear Vegard's law-type behaviour. The interlayer spacing, c, expands on incorporation of bod, with the M–L–M distance, b, in turn shortening. The contraction along b can be explained by the shorter N–N distance in bod than btd, which would predict $b_{btd} - b_{bod} = 0.40$ Å, in quantitative agreement with the fitted value of 0.391(7) Å.[19,20] The significant interlayer expansion cannot be easily rationalised by differences in the size between btd and bod, but seem rather to reflect small differences in the chain tilting angles, though might arise from weaker vdW forces for bod than btd. The near constant a axis suggests that the $NiCl_2$ chain is unperturbed by the differences in Ni–N bonding and that changes in intermolecular forces between bod and btd are not a driving factor. We find no evidence of superlattice reflections indicative of long-range ordering of the bod and btd ligands or structured diffuse scattering from local ordering, though this may be challenging to detect.[21] Having developed this solid-solution series, we then investigated their mechanical compressibility and magnetic properties.

We measured the compressibilities using high pressure synchrotron X-ray powder diffraction (HP-PXRD) at the I15 beamline of Diamond Light Source, using a hydraulic pressure cell to obtain the fine pressure resolution required [Fig. 3].[22] This cell allows measurements from ambient to 0.4 GPa with pressure increments of $\Delta P = 0.02$ GPa. We used silicone oil AP-100 as a pressure transmitting medium,[23] which should be hydrostatic and non-penetrating at these pressures. We investigated here the doped samples synthesised directly using solid-state synthesis because they were more crystalline. The lattice parameters were refined using Pawley refinement. A limited number of impurity peaks were identified and fitted using additional structure free peaks [Section S2.2, Fig. S6–S14, Tables S2–S4, ESI†].

We found no evidence of pressure-induced framework degradation or phase transitions up to 0.4 GPa. The bulk compressibility, B_0, was fitted using the second-order Birch–Murnaghan equation of state.[25,26] Pure $NiCl_2(btd)$ has $B_0 = 18.7(3)$ GPa, with
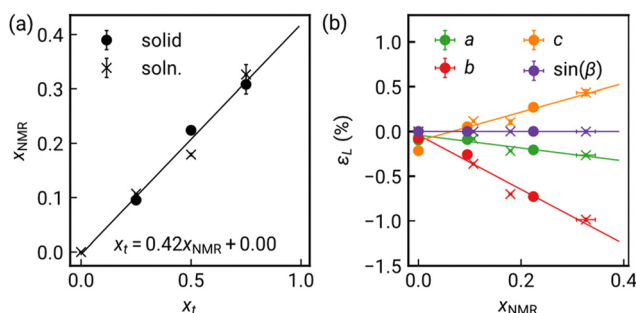

Fig. 2 (a) Determination of x through integration of solution ^{1}H NMR spectra. Linear fit shown. (b) Variation in lattice parameter strain (ε_L) with linear fit. Data point for $x_{NMR} = 0.31$ solid-state excluded due to presence of $NiCl_2 \cdot 6H_2O$ impurity. Circles indicate solid-state samples, crosses solution samples.
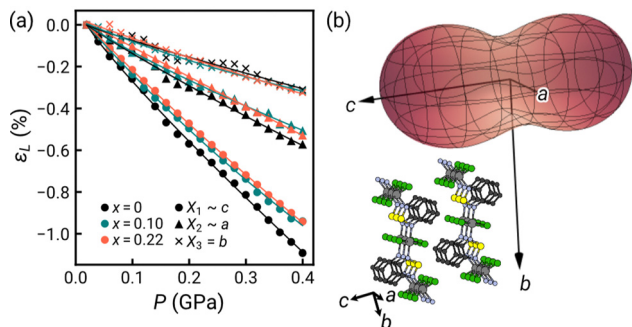
Fig. 3 (a) Linear strain (ε_L) along each principal axis determined through HP-PXRD for solid-state $NiCl_2(btd)_{1-x}(bod)_x$, with compressibility fit by an empirical equation of state.[24] (b) Linear compressibility indicatrix at $P = 0.2$ GPa for $x = 0.22$ (solid) with crystal structure in similar orientation.

the two doped samples both slightly stiffer: $x = 0.10$ has $B_0 = 20.6(3)$ GPa and $x = 0.22$ has $B_0 = 19.96(13)$ GPa [Fig. S5, ESI†]. These values are comparable to those reported for other Ni(II) vdW materials, *e.g.* $Ni(NCS)_2$ $B_0 = 17.0(2)$ GPa,[27] and NiI_2 $B_0 = 27.7(9)$ GPa,[28] and stiffer than $ZnCl_2(3,5$-dichloropyridine)$_2$, $B_0 = 14.52(8)$ GPa, which contains 1D $ZnCl_2$ chains.[29]

Our HP-XRD measurements probe not only the bulk modulus, but also how compressibility varies with direction. The principal compressibilities approximately coincide with the crystallographic axes, although in a monoclinic system the principal strains will not lie in general along the unit cell axes. The compressibility is largest along the interlayer direction, X_1 ($\sim c$) $K_1 = 27.3(3)$ TPa^{-1}. X_2 ($\sim a$) is next stiffest, corresponding to the Ni–Cl–Ni chain direction, $K_2 = 14.8(4)$ TPa^{-1}, with the stiffest direction being the X_3 (b) along the Ni–N–(O/S)–N–Ni bonds direction, $K_3 = 7.7(4)$ TPa^{-1} [Fig. 3 and Table S1, ESI†]. The large compressibility normal to the vdW layers is typical, *e.g.*, $Ni(NCS)_2$ $K_{vdW} = 32.5(2)$ TPa^{-1}. As inorganic materials tend to be less compressible, X_2, with purely inorganic connectivity, might be expected to be the stiffest, but in fact it is nearly twice as soft as X_3, with purely metal–organic connectivity. This is likely because reducing X_3 corresponds to bond compression, whereas the X_2 direction corresponds to bending of the Ni–Cl–Ni angle, although DFT calculations suggest potentially significant π–π-interactions along X_2.[16] This trend is consistent with previous investigations of metal organic materials, *e.g.*, $[CuCl(pyrazine)_2]BF_4$ where the Cu–pyrazine–Cu plane is significantly stiffer than the Cu–Cl–Cu chain,[30] and the plastically deforming $ZnCl_2(3,5$-dichloropyridine)$_2$, where the $ZnCl_2$ chains are as soft as the vdW directions ($K_{ZnCl_2} \approx 23$ TPa^{-1}).

The changes in compressibility on doping are also anisotropic. The interlayer direction becomes notably stiffer, with compressibility dropping to 24.7(4) TPa^{-1} ($x = 0.10$) and 24.70(11) TPa^{-1} ($x = 0.20$). Within the plane, the inorganic X_2 axis becomes slightly stiffer, 12.6(2) TPa^{-1} ($x = 0.10$) and 14.1(3) TPa^{-1} ($x = 0.20$), whereas the organic X_3 axis in fact softens, 8.14(16) TPa^{-1} ($x = 0.10$) and 8.9(4) TPa^{-1} ($x = 0.20$) [Table S1, ESI†]. Organic substitution thus subtly modifies the compressibility of MOMs, as found for MOFs,[31] and hence can change the efficacy of strain tuning, whether in bulk or on surface.[32,33]

We also investigated the magnetic properties of these MOMs for all five solid-solution samples and $NiCl_2(btd)$ [Fig. 4 and Section S3, Fig. S21–S24, Table S7, ESI†]. Our previous work showed $NiCl_2(btd)$ is a canted (weak) ferromagnet due to the noncollinear easy-axes of the paramagnetic Ni^{2+} ions with a canting angle of 9.1(4)°.[16] All our new samples have similar properties: canted magnets with magnetic ordering temperatures, $T_c = 17(1)$ K, and substantial hysteresis [Fig. 4(a), (b), (d) and Table S7, ESI†]. Doping does not greatly affect T_c, despite the substitution of S for O occurring along the superexchange pathway [Fig. 4(c) and Fig. S22, Table S7, ESI†]. Contrastingly, the more bod added, the softer the magnet, with the coercive field, H_c, decreasing by 60% on doping with 33% bod (*i.e.* $x = 0.33$). The reduction in H_c likely arises as bod has both weaker spin–orbit coupling and ligand field, reducing the single-ion anisotropy. It is also possible that the slight differences in tilt angles between $NiCl_2$ chains induced by ligand geometry change the degree of canting, though this is not clearly observed, and the changes in H_c are much larger than predicted by geometry alone.

The observed effect of isovalent substitution on magnetic function is consistent with previous studies: replacing S with Se does not produce large changes in T_c with a 5% reduction for $NiPS_3$,[34] and a 30% increase (1.5 K) for $Co(NCS)_2(pyridine)_2$;[35] but does switch the anisotropy from easy-plane in $NiPS_3$ to easy-axis in $NiPSe_3$.[34] We found larger changes in magnetic properties than in the layered ZIFs, where ligand substituents had
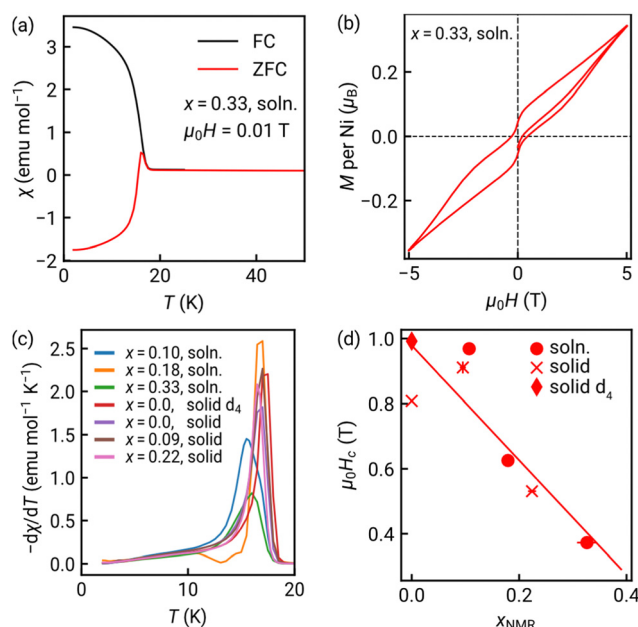

Fig. 4 Magnetic characterisation of the most heavily doped sample ($x = 0.33$, solution). (a) Susceptibility as a function of temperature $\chi(T)$ for samples cooled in magnetic field (FC) and in zero field (ZFC). Negative magnetisation due to small remnant field in magnet. (b) Isothermal magnetisation, $M(H)$, at $T = 2$ K. The variation in magnetic properties with x, (c) ordering temperature T_c with x, shown by the peak in $\frac{d\chi}{dT}$ and (d) variation in coercive field H_c. Linear fit to data shown. Circles indicate solid-state samples (solid), crosses solution sample (soln.), and diamonds solid-state deuterated sample (solid d$_4$).

relatively small effects on both T_c and superexchange.[10,36] The change in coercivity is much larger than previously observed on isovalent substitution in other van der Waals magnets. Pressure can tune noncollinearity in MOMs,[37] and so the combination of mechanical and magnetic tunability we demonstrate suggests that doping will be an effective method to modulate strain switchability.

In conclusion, we demonstrate that ligand solid-solutions achieve fine control over both the mechanical and magnetic properties of vdW MOMs. We report the synthesis of $NiCl_2(btd)_{1-x}(bod)_x$ with an approximately linear dependence of the lattice parameters on ligand substitution. The btd ligand is preferentially incorporated into the structure, likely as it is more electron rich. Investigation of the mechanical properties using HP-PXRD showed that bod stiffens the framework, primarily due to a reduction in interlayer compressibility, as the layers themselves become slightly more compressible. The canted ferromagnetism is retained on doping but there is significant reduction (up to 60%) in coercive field. These results demonstrate that functionalisation of organic ligands can be a valuable way to tune both the magnetic function and pressure-responsiveness of van der Waals metal–organic magnets.

Data availability

Data for this article with analysis scripts available at doi: **https://doi.org/10.17639/nott.7454**. Crystallographic data has been deposited at the CCDC (**https://www.ccdc.cam.ac.uk/structures/**) with reference numbers 2373766, 2373767 and 2377919.†

Conflicts of interest

There are no conflicts to declare.

Notes and references

1 M. Eddaoudi, et al., Science, 2002, **295**, 469–472.
2 X. Kong, et al., Science, 2013, **341**, 882–885.
3 A. D. Burrows, et al., Chem. Commun., 2011, **47**, 3380–3382.
4 S. Horike, et al., Chem. Sci., 2012, **3**, 116–120.
5 C.-C. Cao, et al., J. Am. Chem. Soc., 2019, **141**, 2589–2593.
6 P. Vervoorts, et al., ACS Mater. Lett., 2021, **3**, 1635–1651.
7 A. E. Thorarinsdottir and T. D. Harris, Chem. Rev., 2020, **120**, 8716–8789.
8 L. S. Xie, et al., Chem. Rev., 2020, **120**, 8536–8580.
9 A. Helal, et al., Natl. Sci. Rev., 2017, **4**, 296–298.
10 J. Lopez-Cabrelles, et al., Chem. Sci., 2022, **13**, 842–847.
11 J. Song, et al., Angew. Chem., Int. Ed., 2022, **61**, e202117565.
12 T. Li, et al., Nat. Mater., 2019, 1–6.
13 F. Aribot, et al., ChemRxiv, 2024, preprint, DOI: **10.26434/chemrxiv-2024-rlsf8**.
14 S. Mondal, et al., Phys. Rev. B: Condens. Matter Mater. Phys., 2019, **99**, 180407.
15 C. A. Occhialini, et al., arXiv, 2023, preprint, arXiv:2306.11720, DOI: **10.48550/arXiv.2306.11720**.
16 J. Pitcairn, et al., J. Am. Chem. Soc., 2024, **146**, 19146–19159.
17 G. S. Papaefstathiou, et al., J. Solid State Chem., 2001, **159**, 371–378.
18 B. Morosin, Acta Crystallogr., 1967, **23**, 630–634.
19 T. Suzuki, et al., J. Org. Chem., 2001, **66**, 8954–8960.
20 M. R. Ams, et al., Chem. – Eur. J., 2019, **25**, 323–333.
21 M. L. Robinson, et al., Inorg. Chem., 2020, **59**, 3026–3033.
22 N. J. Brooks, et al., Rev. Sci. Instrum., 2010, **81**, 064103.
23 S. Dissegna, et al., J. Am. Chem. Soc., 2018, **140**, 11581–11584.
24 A. L. Goodwin, et al., Proc. Natl. Acad. Sci. U. S. A., 2008, **105**, 18708–18713.
25 F. Birch, Phys. Rev., 1947, **71**, 809–824.
26 M. Lertkiattrakul, et al., J. Open Source Softw., 2023, **8**, 5556.
27 M. Geers, et al., Phys. Rev. B, 2023, **108**, 144439.
28 M. P. Pasternak, et al., Phys. Rev. Lett., 1990, **65**, 790–793.
29 X. Liu, et al., Nat. Commun., 2021, **12**, 3871.
30 R. Scatena, et al., Inorg. Chem., 2020, **59**, 10091–10098.
31 L. R. Redfern, et al., J. Am. Chem. Soc., 2019, **141**, 4365–4371.
32 D. L. Esteras, et al., Nano Lett., 2022, **22**, 8771–8778.
33 J. Cenker, et al., Nat. Nanotechnol., 2022, **17**, 256–261.
34 R. Basnet, et al., Phys. Rev. Res., 2022, **4**, 023256.
35 T. Neumann, et al., Chem. Commun., 2019, **55**, 2652–2655.
36 J. López-Cabrelles, et al., J. Am. Chem. Soc., 2021, **143**, 18502–18510.
37 I. E. Collings, et al., Phys. Chem. Chem. Phys., 2018, **20**, 24465–24476.